

Research
Green Chemical Engineering—Article

An Evaluation of Metronidazole Degradation in a Plasma-Assisted Rotating Disk Reactor Coupled with TiO₂ in Aqueous Solution



Yong Cai ^{a,b}, Guang-Wen Chu ^{a,b,*}, Yong Luo ^{b,*}, Meng-Jun Su ^{a,b}, Bao-Ju Wang ^{a,b}, Bao-Chang Sun ^b, Jian-Feng Chen ^{a,b}

^a State Key Laboratory of Organic-Inorganic Composites, Beijing University of Chemical Technology, Beijing 100029, China

^b Research Center of the Ministry of Education for High-Gravity Engineering and Technology, Beijing University of Chemical Technology, Beijing 100029, China

ARTICLE INFO

Article history:

Received 21 July 2019

Revised 18 December 2019

Accepted 8 March 2020

Available online 7 October 2021

Keywords:

Plasma-assisted rotating disk reactor

Pulsed discharge

Metronidazole

Degradation

TiO₂

ABSTRACT

Pollution involving pharmaceutical components in bodies of water is an increasingly serious environmental issue. Plasma discharge for the degradation of antibiotics is an emerging technology that may be relevant toward addressing this issue. In this work, a plasma-assisted rotating disk reactor (plasma-RDR) and a photocatalyst—namely, titanium dioxide (TiO₂)—were coupled for the treatment of metronidazole (MNZ). Discharge uniformity was improved by the use of a rotating electrode in the plasma-RDR, which contributed to the utilization of ultraviolet (UV) light radiation in the presence of TiO₂. The experimental results showed that the degradation efficiency of MNZ and the concentration of generated hydroxyl radicals respectively increased by 41% and 2.954 mg·L⁻¹ as the rotational speed increased from 0 to 500 r·min⁻¹. The synergistic effect of plasma-RDR plus TiO₂ on the generation of hydroxyl radicals was evaluated. Major intermediate products were identified using three-dimensional (3D) excitation emission fluorescence matrices (EEFMs) and liquid chromatography–mass spectrometry (LC-MS), and a possible degradation pathway is proposed herein. This plasma-catalytic process has bright prospects in the field of antibiotics degradation.

© 2021 THE AUTHORS. Published by Elsevier LTD on behalf of Chinese Academy of Engineering and Higher Education Press Limited Company. This is an open access article under the CC BY-NC-ND license (<http://creativecommons.org/licenses/by-nc-nd/4.0/>).

1. Introduction

Metronidazole (1-hydroxyethyl-2-methyl-5-nitroimidazole; MNZ), one of the most common nitroimidazole-based antibiotic drugs, is widely used to treat infections by anaerobic bacteria and protozoa, such as *Trichomonas* and *Giardia lamblia* [1,2]. MNZ is also added to poultry and fish feed to eliminate parasites. More importantly, MNZ possesses potential biological carcinogenicity and mutagenicity [3–5]. As a pharmaceutical substance and a potential carcinogen, MNZ tends to accumulate in aquatic environments, resulting in the pollution of surface water and groundwater [6–8]. Due to the toxicity and high water solubility of MNZ [9], the elimination of this compound from the environment has become a significant issue. Hence, it is imperative to exploit new techniques to remove MNZ pollution effectively.

Various technologies have been reported to degrade MNZ, including ultraviolet (UV) irradiation [10], Fenton/UV [11], heterogeneous photocatalysis [12], nanoscale zero-valent metal reduction [13], and adsorption/bio-adsorption on activated carbon [14]. Aside from these methods, non-thermal plasma generated by electrical discharge in liquid or at the gas–liquid interface, inducing a variety of chemical and physical effects *in situ*, has attracted a considerable amount of attention [15]. These effects include intense UV radiation, shockwaves, high-energy electrons, and, especially, the formation of various reactive oxygen species (i.e., ozone, hydrogen peroxide, hydroxyl radicals, and perhydroxyl radicals) [16]. Therefore, plasma discharge has been widely used for the removal of different antibiotics from aqueous solutions, such as pentoxyfylline [17], three β-lactam antibiotics [18], and carbamazepine [19]. However, there are few reports on the degradation of MNZ by plasma discharge, even though this technology may be efficiently utilized as an environmentally friendly technology for MNZ degradation.

Diverse plasma-discharge modes have been studied with different electrode geometries (e.g., needle–needle, needle–plate, and

* Corresponding authors.

E-mail addresses: chugw@mail.buct.edu.cn (G.-W. Chu), luoyong@mail.buct.edu.cn (Y. Luo).

wire–plate) for degrading different types of organic compounds [20]. Recently, a plasma-assisted rotating disk reactor (plasma-RDR), which involves the coupled fields of plasma and high gravity, was innovatively developed to enhance the degradation efficiency of organic dye compounds [21]. The main advantages of the plasma-RDR are as follows: ① Because of the strong centrifugal force, a micron-liquid film is obtained, which favors the renewal of the plasma–liquid interface and thus increases the utilization of the hydroxyl radicals; and ② all the involved energies produced by plasma discharge can act directly on the liquid film.

Titanium dioxide (TiO_2) is regarded as an ideal photocatalyst due to its high charge separation efficiency and its effective utilization of UV light radiation [22,23]. During photocatalytic processes, reactive oxygen species—which are key active sources in the photocatalytic degradation of antibiotics—can be generated [24–26]. Thus, a high degradation efficiency of MNZ can be expected in a plasma-RDR coupled with TiO_2 .

This work studied the enhancement of the degradation efficiency of MNZ. The effects of the operating conditions on the energy yield were evaluated, and a correlation between the energy yield and the operating conditions in the plasma-RDR was obtained. A plasma-RDR and a TiO_2 photocatalyst were coupled in order to enhance the degradation efficiency of MNZ. The structure and morphology, catalytic performance, and reusability of the TiO_2 before and after discharge were systematically characterized. Three-dimensional (3D) excitation emission fluorescence matrix (EEFM) spectroscopy was selected to qualitatively investigate the concentration of MNZ. Major degradation intermediates of MNZ were identified, and a possible degradation pathway for MNZ was then proposed.

2. Experimental method and procedure

2.1. Plasma generator

The input voltage of the plasma generator (Beijing Ruiant Technology Co., Ltd., China) was an alternating current (AC) pulse signal. The voltage and current in the plasma-RDR were measured by a Rigol PVP2150 high-voltage probe (RIGOL Technologies Co., Ltd., USA) and a Cybertek CP0030A current probe (Shenzhen Zhiyong Electronics Co., Ltd., China) connected to a Tektronix TDS3032C oscilloscope (Tektronix, Inc., USA). The average power of the plasma-RDR, as determined by the voltage and current waveforms, can be calculated using Eq. (1):

$$P = \left(\int_0^T U \cdot Idt \right) \cdot f \quad (1)$$

where P is the average power, U is the instantaneous voltage, I is the instantaneous current, T is the pulse duration, and f is the pulse repetition frequency. Considering previous reports on discharge characteristics for the degradation of rhodamine B, the peak voltage (V_{pp}) and electrode gap (d) were set as 44 kV and 8 mm, respectively [21].

Energy yield, was adopted to illustrate the energy consumption required to degrade MNZ, as calculated by Eq. (2) [27]:

$$Y = \frac{C_0 \cdot V \cdot \eta}{100 \cdot P \cdot t} \quad (2)$$

where Y is the energy yield ($\text{g} \cdot (\text{kW} \cdot \text{h})^{-1}$), C_0 is the initial concentration of MNZ ($\text{g} \cdot \text{L}^{-1}$), V is the volume of MNZ solution (L), η is the degradation efficiency, and t is the treatment time (h).

2.2. Experimental procedure

Fig. 1 shows the experimental setup for the degradation of MNZ. Deionized water containing MNZ and oxygen was fed into the plasma-RDR by gas–liquid co-current flow. In our previous research, we provided details on plasma-RDR with gas–liquid co-current flow [28]. Oxygen with a flow rate of $0.5 \text{ m}^3 \cdot \text{h}^{-1}$ was fed into the plasma-RDR for 30 min before the start of the experiments in order to generate more reactive oxygen species. Then deionized water containing MNZ was introduced into the plasma-RDR, flowed radially outward through the rotating low-voltage electrode, was collected in a fluid reservoir below, and was circulated into the plasma-RDR by means of a pump. The MNZ solution was sampled every 20 min at the liquid outlet.

2.3. Analytical methods

The concentration of MNZ was determined by measuring the absorption intensity of MNZ at the wavelength of 318 nm with a UV spectrophotometer (U-2800, Hitachi, Japan) [7,29]. The typical absorption spectra of MNZ is shown in **Fig. 2**. The efficiency with which the MNZ solution was degraded (herein referred to as the degradation efficiency of MNZ) was calculated based on the following equation:

$$\eta = \frac{C_0 - C}{C_0} \times 100\% \quad (3)$$

where C is the final concentrations of MNZ.

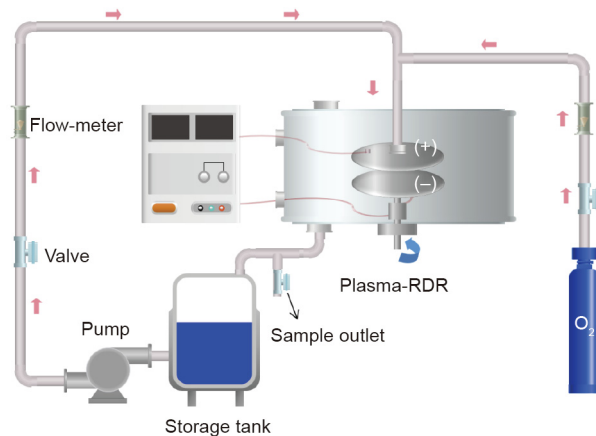


Fig. 1. Schematic diagram of the experimental setup.

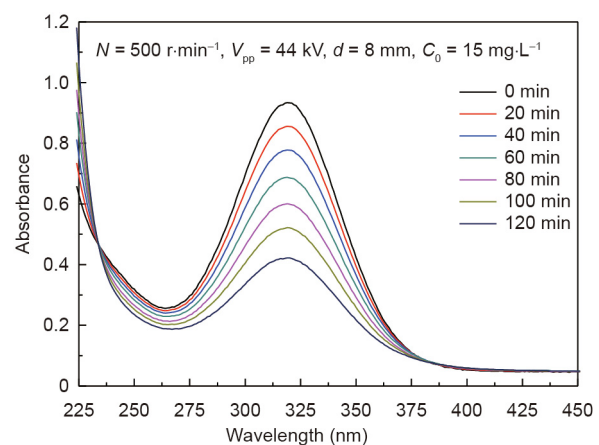


Fig. 2. Absorption spectra of MNZ solution before and after treatment. N : rotational speed.

The crystal structure of TiO_2 was analyzed by X-ray diffraction (XRD; D/max 2550, Rigaku Co., Japan) and the angular range of 2θ was from 10° to 80° . The processes were carried out at 40kV and 50mA .

Intermediates of MNZ degradation during the plasma treatment process were identified through liquid chromatography–mass spectrometry (LC-MS; Xevo G2 QToF, Waters Co., USA).

3. Results and discussion

3.1. Enhanced degradation performance of plasma-RDR

As shown in Fig. 3(a), the effect of rotational speed (N) on the degradation efficiency of MNZ was evaluated. The role of rotation on MNZ degradation was found to be significant. The degradation efficiency of MNZ was merely 9.5% at $0\text{r}\cdot\text{min}^{-1}$ and increased by 24% at $400\text{r}\cdot\text{min}^{-1}$. When the rotational speed was increased to $500\text{r}\cdot\text{min}^{-1}$, the degradation efficiency was as high as 50.2% . The degradation efficiency of MNZ changed slightly when the rotational speed exceeded $500\text{r}\cdot\text{min}^{-1}$. Due to the strong centrifugal force, the plasma–liquid interface renewal was clearly enhanced, followed by improvement in the utilization of the hydroxyl radicals. As shown in Fig. 3(b), the concentration of hydroxyl radicals generated in the plasma-RDR increased by $2.954\text{ mg}\cdot\text{L}^{-1}$ when the rotational speed was increased from 0 to $500\text{r}\cdot\text{min}^{-1}$.

3.2. Investigation of the degradation efficiency and energy yield of the plasma-RDR

3.2.1. Effects of operating conditions on degradation efficiency

Fig. 4 illustrates the effects of the operating conditions on the degradation efficiency. The effects of the initial concentration of

MNZ, pulse repetition frequency, and volume of solution were evaluated when the rotational speed and liquid flow rate were respectively set as $500\text{r}\cdot\text{min}^{-1}$ and $80\text{ L}\cdot\text{h}^{-1}$.

As shown in Fig. 4(a), the degradation efficiency of MNZ decreased with the increase of the initial concentration of MNZ. When there was a lower concentration of MNZ, the initial degradation efficiency was higher. The final degradation efficiency reached 73.1% and 68.1% for MNZ concentrations of $5.0\text{ mg}\cdot\text{L}^{-1}$ and $7.5\text{ mg}\cdot\text{L}^{-1}$, respectively. However, the degradation efficiency was only 54.8% for an MNZ concentration of $15\text{ mg}\cdot\text{L}^{-1}$. Thus, it can be reasonably speculated that the degradation of high concentrations of MNZ requires more energy and a longer treatment time. Hence, a concentration of $7.5\text{ mg}\cdot\text{L}^{-1}$ was selected as the experimental condition for subsequent experiments using only plasma-RDR.

Pulse repetition frequency was selected to change the average power. Fig. 4(b) shows that the degradation efficiency of MNZ increased with an increase in pulse repetition frequency. The degradation efficiency increased slightly when the pulse repetition frequency increased from 200 to 240 Hz . The experimental results can be explained as follows: At higher pulse repetition frequencies, the electrical condenser had insufficient time to fully recharge; therefore, the energy injected to the plasma-RDR decreased [30].

The volume of treated solution affected the capacity to degrade MNZ. As shown in Fig. 4(c), the degradation efficiency reached 73% with a solution volume of 1.75 L and then decreased slightly for volumes ranging from 1.75 to 2.25 L . The degradation efficiency decreased by 20.4% with an increase in the solution volume from 2.25 to 2.50 L . When the volume of the solution exceeded 2.25 L , the capacity to treat MNZ was seriously restricted. Based on these experimental results, a solution volume of 2.00 L was selected for the subsequent experiments.

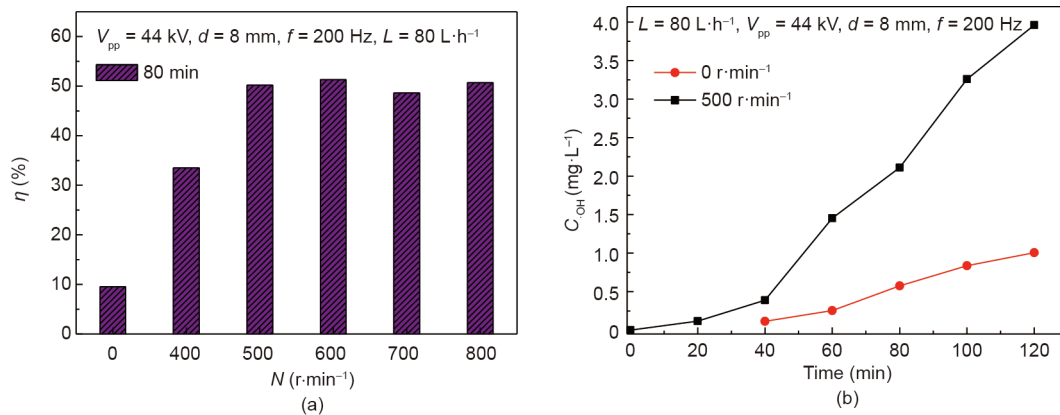


Fig. 3. Enhanced (a) degradation efficiency of MNZ and (b) production of hydroxyl radicals in the plasma-RDR. L : liquid flow rate.

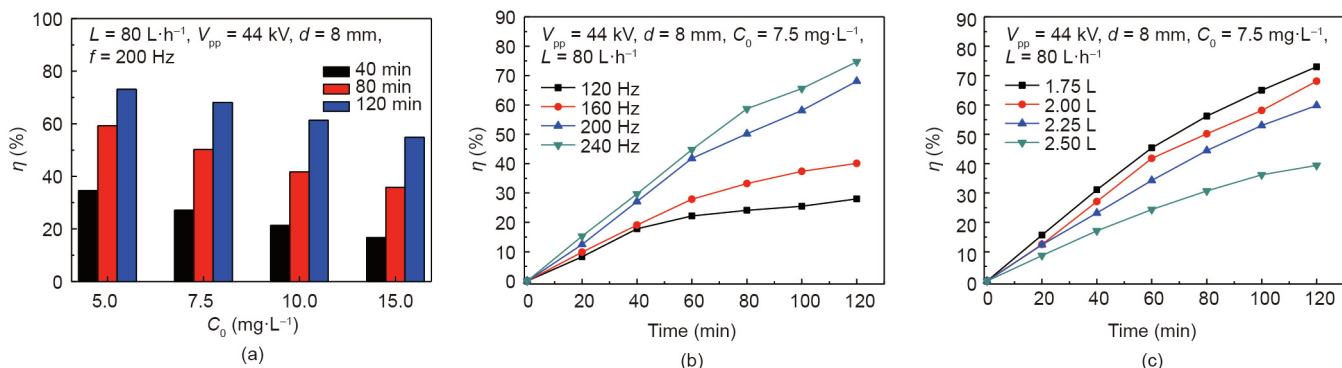


Fig. 4. Effects of (a) initial concentration of MNZ, (b) pulse repetition frequency, and (c) volume of solution on the degradation efficiency of MNZ.

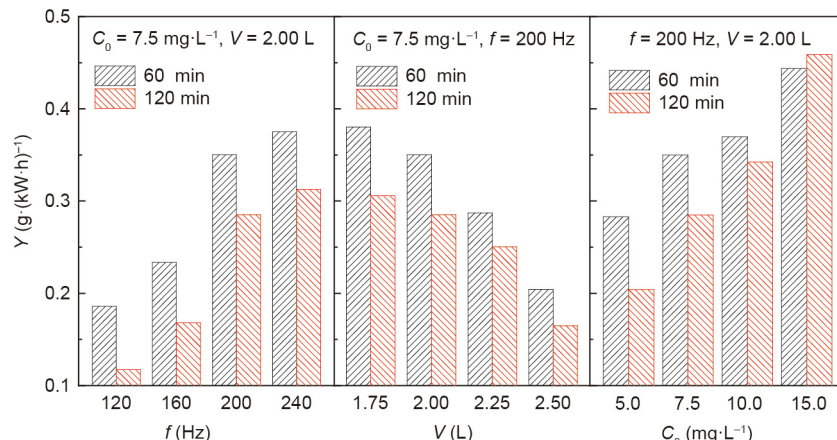


Fig. 5. Effects of operating conditions on the energy yield of the plasma-RDR.

3.2.2. Effects of operating conditions on energy yield and a correlation between energy yield and operating conditions

Degradation efficiency can be illustrated by the quantity of MNZ decomposed per unit of energy (i.e., yield). The energy yield relies on the type of plasma reactor, the initial concentration, and the characteristics of the compound [31]. Approximately 70% degradation was obtained within 120 min using the starting parameters mentioned earlier. Fig. 5 presents detailed data on the energy yield under different operating conditions. It was noted that the energy yield as a function of time decreased and changed with the pulse repetition frequency, the volume of solution, and the initial concentration of MNZ. When the pulse repetition frequency was increased from 120 to 240 Hz, the energy yield increased from 0.19 to 0.38 g·(kW·h)⁻¹ for an MNZ concentration of 7.5 mg·L⁻¹ within 60 min. Similarly, with an increase in the initial concentration of MNZ from 5.0 to 15.0 mg·L⁻¹, the energy yield increased from 0.28 to 0.44 g·(kW·h)⁻¹ within 60 min. When the volume of solution was increased from 1.75 to 2.50 L, the energy yield decreased from 0.38 to 0.20 g·(kW·h)⁻¹ for a concentration of 7.5 mg·L⁻¹ within 60 min.

Based on the above experimental data, a correlation between the energy yield, Y , and the other operating conditions in a plasma-RDR was proposed, as shown in Eq. (4):

$$Y = 4.39 \times 10^{-4} f^{1.213} V^{-1.465} \times C_0^{0.587} \times t^{0.228} \quad (4)$$

It can be seen that the pulse repetition frequency and the volume of the solution have a greater impact on energy yield, whereas the treatment time has the smallest effect among the operating conditions. Fig. 6 shows the values of energy yield obtained experimen-

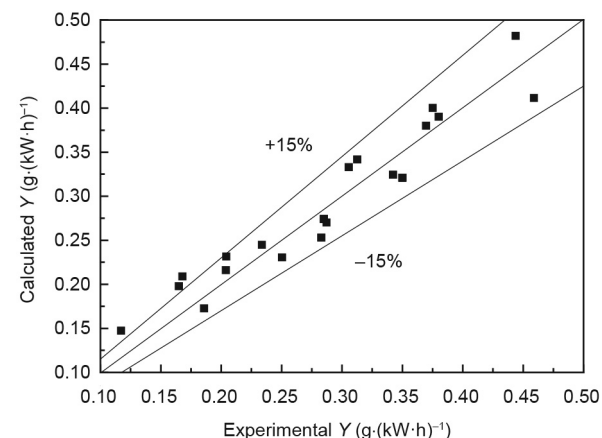


Fig. 6. Comparison of the calculated and experimental energy yield, Y .

tally versus the values predicted by Eq. (4), which exhibits a deviation of $\pm 15\%$.

3.3. Degradation of MNZ in a plasma-RDR coupled with TiO_2

3.3.1. Effect of TiO_2 additive amount

The effect of the amount of TiO_2 added to the solution in the plasma-RDR on the degradation efficiency of MNZ is exhibited in Fig. 7(a). The experiments were conducted with a liquid flow rate of 80 L·h⁻¹, an initial MNZ concentration of 15.0 mg·L⁻¹, and a

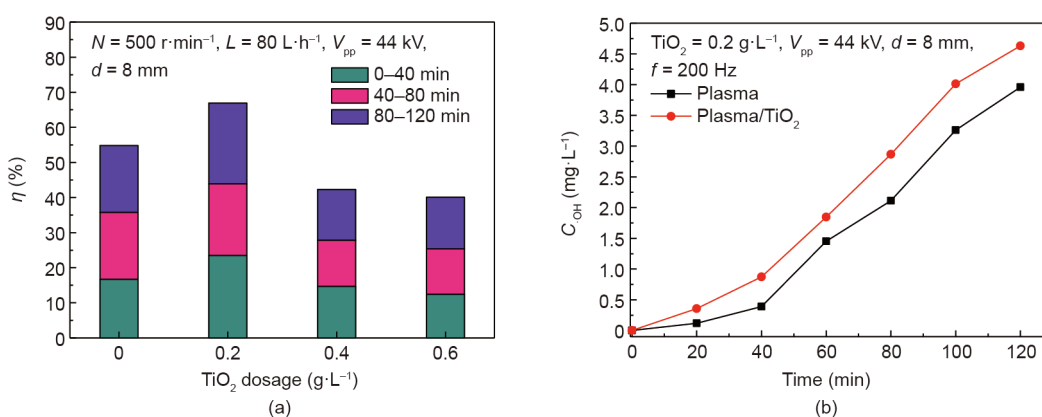


Fig. 7. Effects of TiO_2 dosage on (a) degradation efficiency of MNZ and (b) production of hydroxyl radicals.

pulse repetition frequency of 200 Hz. The experimental results revealed that $0.2 \text{ g} \cdot \text{L}^{-1}$ was the optimal TiO_2 additive amount for a higher degradation efficiency of MNZ. When the additive amount of TiO_2 exceeded this value, the degradation efficiency induced by the plasma discharge decreased. It can be understood that an increase in TiO_2 particles improved the number of photons that were absorbed. When the concentration of TiO_2 particles exceeded $0.2 \text{ g} \cdot \text{L}^{-1}$, light scattering and screening effects ensued. Excessive opacity of the suspension restricted the TiO_2 nanoparticles that were furthest in from being irradiated [32]. Due to the scattering and screening effects, the catalytic activity of the TiO_2 particles was reduced [33]. Particle aggregation always occurs at high concentrations [34]. The optimum amount of TiO_2 for degrading MNZ was deemed to be $0.2 \text{ g} \cdot \text{L}^{-1}$. Furthermore, the synergistic effect of the plasma-RDR plus TiO_2 was significant in generating hydroxyl radicals. As shown in Fig. 7(b), the concentration of hydroxyl radicals increased by $0.671 \text{ mg} \cdot \text{L}^{-1}$ within 120 min with the aid of the TiO_2 photocatalyst.

3.3.2. Characteristics of TiO_2 before and after plasma discharge

To examine the morphology and structural features of the TiO_2 particles before and after discharge in the plasma-RDR, scanning electron microscope (SEM) and transmission electron microscope (TEM) patterns of TiO_2 were obtained for comparison, as shown in Figs. 8(a)–(f). Figs. 8(a) and (c) respectively show the SEM and TEM images of the original TiO_2 particles, from which it can be clearly concluded that many of the TiO_2 particles were irregularly spherical. After discharge for the treatment of MNZ, the surface morphology of the TiO_2 particles (Figs. 8(b) and (d)) was found to be almost identical to that of the original TiO_2 particles. Figs. 8(e) and (f) indicate nearly the same plane spacing, which was approximately 0.350 nm both before and after discharge, corresponding to the spacing of the (101) plane of anatase TiO_2 [35,36].

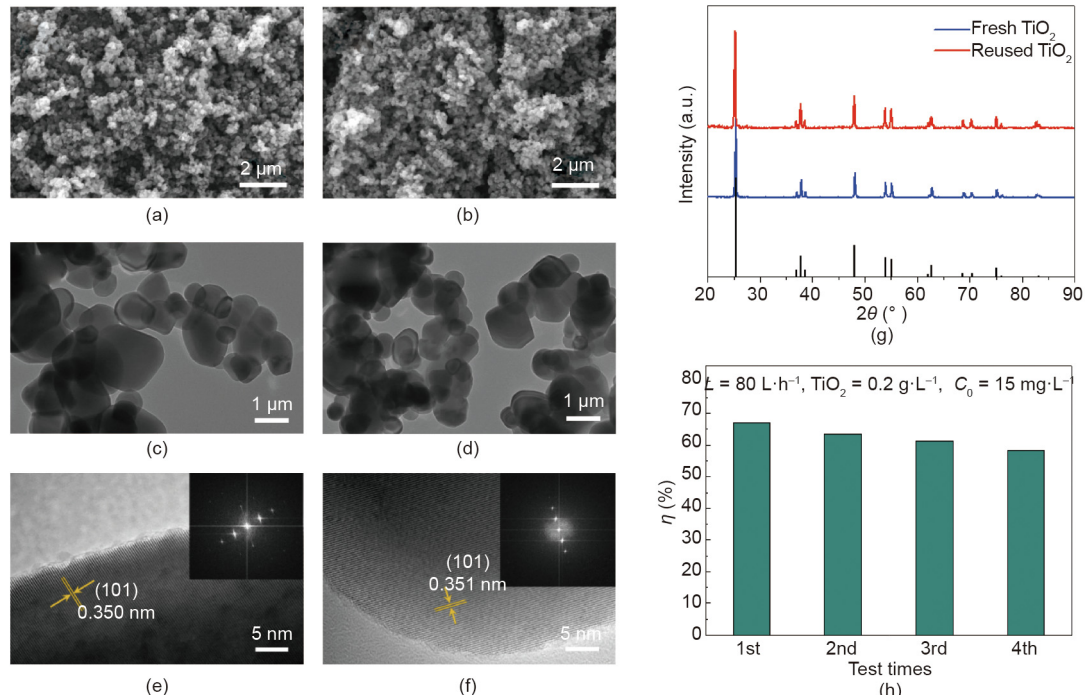


Fig. 8. SEM images of TiO_2 (a) before and (b) after discharge; TEM images of TiO_2 (c) before and (d) after discharge; high-resolution transmission electron microscope (HRTEM) images of TiO_2 (e) before and (f) after discharge; (g) XRD patterns of TiO_2 before and after discharge; (h) cycling tests of TiO_2 particles.

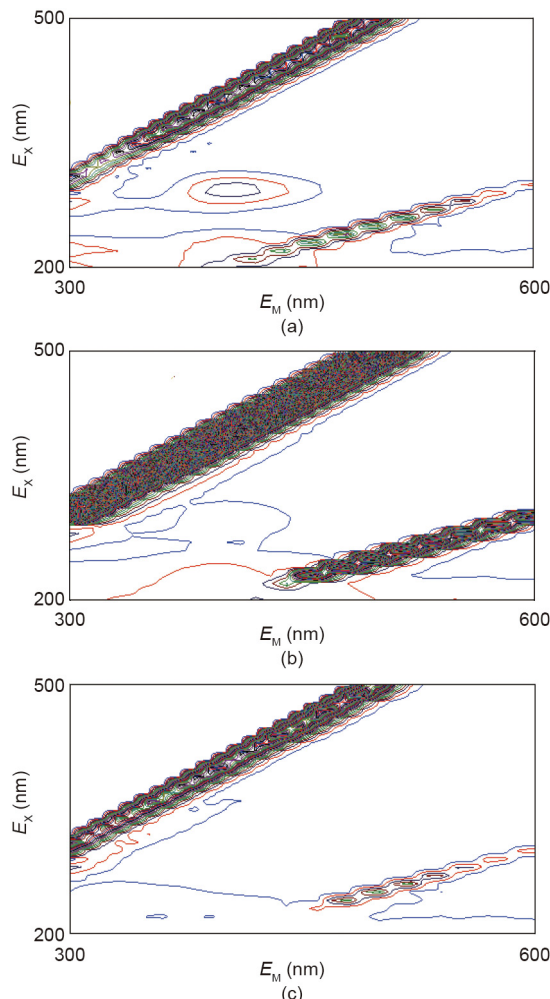


Fig. 9. 3D EEFMs of MNZ solution after treatment times of (a) 0 min, (b) 60 min, and (c) 120 min in the plasma-RDR/TiO₂ system. E_x : excitation wavelength; E_m : emission wavelength.

complex. Heterocyclic intermediates were mainly formed by hydroxylation with denitration (No. 3 and No. 5), oxidation of the lateral N-ethanol to an N-acetic acid group (No. 2 and No. 3), and the loss of these lateral groups (No. 4 and No. 5). It is

Table 1
Intermediates identified by LC-MS.

No.	Molecular weight	Molecular formula	Chemical structure
1	171	C ₆ N ₃ H ₉ O ₃	
2	185	C ₆ N ₃ H ₇ O ₄	
3	156	C ₆ N ₂ H ₈ O ₃	
4	127	C ₄ N ₃ H ₅ O ₂	
5	98	C ₄ N ₂ H ₆ O	

anticipated that further breakage of the imidazole portion and oxidation of the resulting linear compounds would produce a mixture of short linear aliphatic carboxylic acids. The presence of oxalic, oxamic, formic, and acetic acids was corroborated by high-performance liquid chromatography (HPLC) analysis [38,39]. These aliphatic acids can be mineralized into CO₂ and H₂O. According to the above experimental results, a possible degradation pathway is proposed, as shown in Fig. 10.

3.5. Degradation mechanism of MNZ in the plasma-RDR/TiO₂ system

Based on the experimental results described above, a schematic diagram of the MNZ degradation mechanism by the plasma-RDR/TiO₂ system is exhibited in Fig. 11. UV-visible light generated by the plasma-RDR induced TiO₂ particles and caused the separation of electron-hole pairs. The produced h⁺ was able to react with H₂O and OH⁻ to form ·OH. The generated conduction electrons were trapped by both the O₂ and the O₃ produced by the discharge, further generating ·OH. The produced ·OH by means of photocatalysis, together with the formed reactive oxygen species by plasma discharge, jointly reacted with MNZ to produce intermediates.

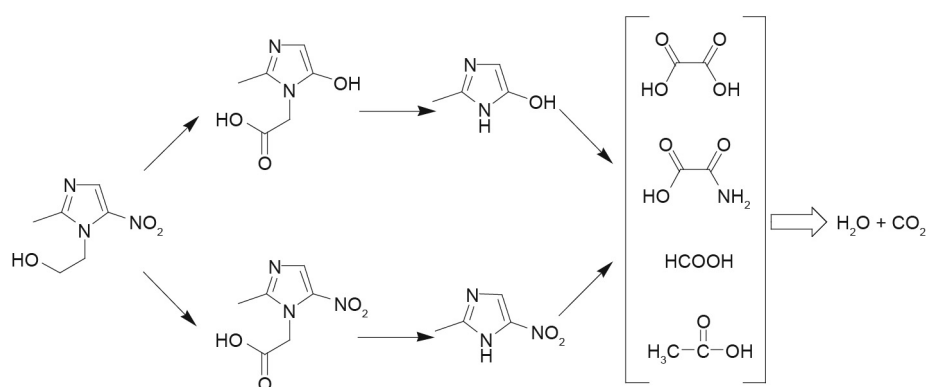


Fig. 10. Possible degradation pathway of MNZ in the plasma-RDR/TiO₂ system.

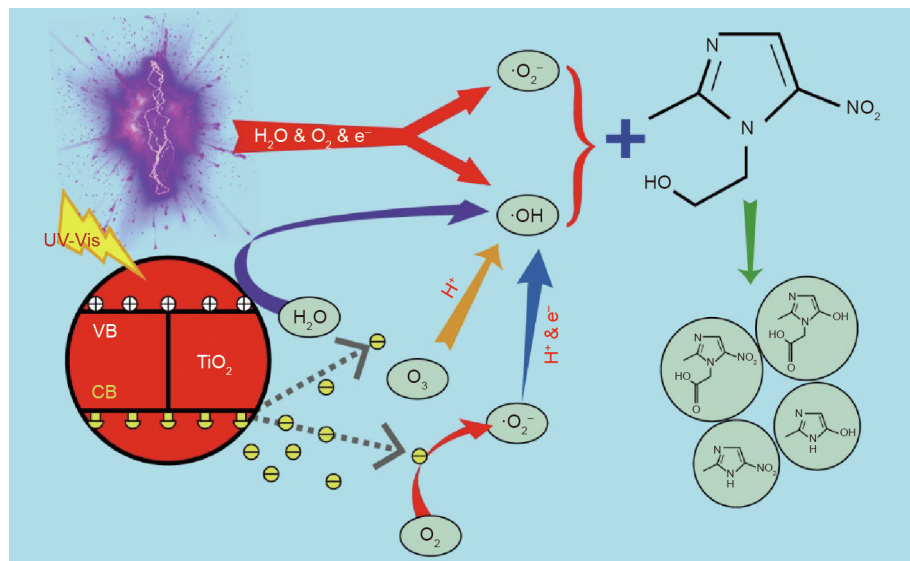


Fig. 11. Degradation mechanism of MNZ in the plasma-RDR/TiO₂ system. UV-Vis: ultraviolet-visible; VB: valence band; CB: conduction band.

4. Conclusions

This work studied the degradation of MNZ in aqueous solution. The degradation efficiency of MNZ and the concentration of hydroxyl radicals generated in the plasma-RDR respectively increased by 41% and 2.954 mg·L⁻¹ with an increase in the rotational speed from 0 to 500 r·min⁻¹. A higher pulse repetition frequency favored the degradation efficiency, whereas a higher initial concentration of MNZ and a greater volume of MNZ solution were unfavorable to the degradation efficiency. Based on the experimental data, the energy yield was calculated and a correlation was proposed. The deviation between the predicted values and the experimental data was within ±15%. The enhanced degradation performance of the plasma-RDR plus TiO₂ was significant, as the concentration of hydroxyl radicals increased by 0.671 mg·L⁻¹ within 120 min. 3D EEFMs and LC-MS demonstrated that the conjugated heterocyclic structures of MNZ were destroyed and small molecules were produced. The plasma-RDR/TiO₂ system is thus a promising technology for antibiotic wastewater treatment.

Acknowledgments

This work was supported by the National Natural Science Foundation of China (21725601).

Compliance with ethics guidelines

Yong Cai, Guang-Wen Chu, Yong Luo, Meng-Jun Su, Bao-Ju Wang, Bao-Chang Sun, and Jian-Feng Chen declare that they have no conflict of interest or financial conflicts to disclose.

References

- [1] Chatzitakis A, Berberidou C, Paspaltsis I, Kyriakou G, Sklaviadis T, Poulios I. Photocatalytic degradation and drug activity reduction of Chloramphenicol. *Water Res* 2008;42(1–2):386–94.
- [2] Dong S, Li Y, Sun J, Yu C, Li Y, Sun J. Facile synthesis of novel ZnO/RGO hybrid nanocomposites with enhanced catalytic performance for visible-light-driven photodegradation of metronidazole. *Mater Chem Phys* 2014;145(3):357–65.
- [3] Chacko M, Bhide SV. Carcinogenicity, perinatal carcinogenicity and teratogenicity of low dose metronidazole (MNZ) in Swiss mice. *J Cancer Res Clin Oncol* 1986;112(2):135–40.
- [4] Legator M, Connor T, Stoeckel M. Detection of mutagenic activity of metronidazole and niridazole in body fluids of humans and mice. *Science* 1975;188(4193):1118–9.
- [5] Bendesky A, Menéndez D, Ostrosky-Wegman P. Is metronidazole carcinogenic? *Mutat Res* 2002;511(2):133–44.
- [6] Daeseleire E, De Ruyck H, Van Renterghem R. Rapid confirmatory assay for the simultaneous detection of ronidazole, metronidazole and dimetridazole in eggs using liquid chromatography-tandem mass spectrometry. *Analyst* 2000;125(9):1533–5.
- [7] Dong SY, Sun JY, Li YK, Yu CF, Li YH, Sun JH. ZnSnO₃ hollow nanospheres/reduced graphene oxide nanocomposites as high-performance photocatalysts for degradation of metronidazole. *Appl Catal B* 2014;144:386–93.
- [8] De Ruyck H, Daeseleire E, De Ridder H, Van Renterghem R. Liquid chromatographic-electrospray tandem mass spectrometric method for the determination of mebendazole and its hydrolysed and reduced metabolites in sheep muscle. *Anal Chim Acta* 2003;483(1–2):111–23.
- [9] Cheng W, Yang M, Xie Y, Fang Z, Nan J, Tsang PE. Electrochemical degradation of the antibiotic metronidazole in aqueous solution by the Ti/SnO₂–Sb–Ce anode. *Environ Technol* 2013;34(21):2977–87.
- [10] Prados-Joya G, Sánchez-Polo M, Rivera-Utrilla J, Ferro-garcía M. Photodegradation of the antibiotics nitroimidazoles in aqueous solution by ultraviolet radiation. *Water Res* 2011;45(1):393–403.
- [11] Shemer H, Kunukcu YK, Linden KG. Degradation of the pharmaceutical metronidazole via UV, Fenton and photo-Fenton processes. *Chemosphere* 2006;63(2):269–76.
- [12] Farzadkia M, Esrafilii A, Baghapour MA, Shahamat YD, Okhovat N. Degradation of metronidazole in aqueous solution by nano-ZnO/UV photocatalytic process. *Desalin Water Treat* 2014;52(25–27):4947–52.
- [13] Fang ZQ, Chen JH, Qiu XH, Qiu XQ, Cheng W, Zhu LC. Effective removal of antibiotic metronidazole from water by nanoscale zero-valent iron particles. *Desalination* 2011;268(1–3):60–7.
- [14] Vertzoni M, Carlsson A, Abrahamsson B, Goumas K, Reppas C. Degradation kinetics of metronidazole and olsalazine by bacteria in ascending colon and in feces of healthy adults. *Int J Pharm* 2011;413(1–2):81–6.
- [15] Shang KF, Wang XJ, Li J, Wang H, Lu N, Jiang N, et al. Synergetic degradation of acid orange 7 (AO7) dye by DBD plasma and persulfate. *Chem Eng J* 2017;311:378–84.
- [16] Wang B, Dong B, Xu M, Chi CM, Wang C. Degradation of methylene blue using double-chamber dielectric barrier discharge reactor under different carrier gases. *Chem Eng Sci* 2017;168:90–100.
- [17] Magureanu M, Mandache NB, Parvulescu VI. Degradation of pharmaceutical compounds in water by non-thermal plasma treatment. *Water Res* 2015;81(11):124–36.
- [18] Magureanu M, Piroi D, Mandache NB, David V, Medvedovic A, Bradu C, et al. Degradation of antibiotics in water by non-thermal plasma treatment. *Water Res* 2011;45(11):3407–16.
- [19] Krause H, Schweiger B, Schuhmacher J, Scholl S, Steinfeld U. Degradation of the endocrine disrupting chemicals (EDCs) carbamazepine, clofibric acid, and iopromide by corona discharge over water. *Chemosphere* 2009;75(2):163–8.
- [20] Ashmarin GV, Lelevkin VM, Tokarev AV. Development of a linear corona torch discharge. *Plasma Phys Rep* 2002;28(10):866–70.
- [21] Cai Y, Luo Y, Sun BC, Fan TX, Chu GW, Chen JF. A novel plasma-assisted rotating disk reactor: enhancement of degradation efficiency of rhodamine B. *Chem Eng J* 2019;377:119897.

- [22] Xiao M, Wang SC, Thaweesak S, Luo B, Wang LZ. Tantalum (oxy)nitride: narrow bandgap photocatalysts for solar hydrogen generation. *Engineering* 2017;3(3):365–78.
- [23] Hao XL, Zhou MH, Zhang Y, Lei LC. Enhanced degradation of organic pollutant 4-chlorophenol in water by non-thermal plasma process with TiO₂. *Plasma Chem Plasma Process* 2006;26(5):455–68.
- [24] Wang K, Li Y, Zhang G, Li J, Wu XY. 0D Bi nanodots/2D Bi₃NbO₇ nanosheets heterojunctions for efficient visible light photocatalytic degradation of antibiotics: enhanced molecular oxygen activation and mechanism insight. *Appl Catal B* 2019;240:39–49.
- [25] Li J, Li Y, Zhang GK, Huang HX, Wu XY. One-dimensional/two-dimensional core-shell-structured Bi₂O₄/BiO_{2-x} heterojunction for highly efficient broad spectrum light-driven photocatalysis: faster interfacial charge transfer and enhanced molecular oxygen activation mechanism. *ACS Appl Mater Interfaces* 2019;11(7):7112–22.
- [26] Wang K, Li J, Zhang GK. Ag-bridged Z-scheme 2D/2D Bi₅FeTi₃O₁₅/g-C₃N₄ heterojunction for enhanced photocatalysis: mediator-induced interfacial charge transfer and mechanism insights. *ACS Appl Mater Interfaces* 2019;11(31):27686–96.
- [27] Zhao S, Hao CJ, Xu D, Wen YY, Qiu J, Liu KF. Effect of electrical parameters on energy yield of organic pollutant degradation in a dielectric barrier discharge reactor. *IEEE Trans Plasma Sci* 2017;45(6):1043–50.
- [28] Cai Y, Wu XS, Luo Y, Su MJ, Chu GW, Sun BC, et al. Plasma-assisted rotating disk reactor toward disinfection of aquatic microorganisms. *Ind Eng Chem Res* 2019;58(31):13977–86.
- [29] Galmier MJ, Frasey AM, Bastide M, Beyssac E, Petit J, Aiache JM, et al. Simple and sensitive method for determination of metronidazole in human serum by high-performance liquid chromatography. *J Chromatogr B* 1998;720(1–2):239–43.
- [30] Zhang YZ, Zheng JT, Qu XF, Chen HG. Design of a novel non-equilibrium plasma-based water treatment reactor. *Chemosphere* 2008;70(8):1518–24.
- [31] Magureanu M, Piroi D, Ghirardi F, Mandache NB, Parvulescu V. Decomposition of methylene blue in water by corona discharges. *Plasma Chem Plasma Process* 2008;28(6):677–88.
- [32] Rahman MA, Munir M. Photocatalysed degradation of two selected pesticide derivatives, dichlorvos and phosphamidon, in aqueous suspensions of titanium dioxide. *Desalination* 2005;181(1–3):161–72.
- [33] Lea J, Adesina AA. The photo-oxidative degradation of sodium dodecyl sulphate in aerated aqueous TiO₂ suspension. *J Photoch Photobio A* 1998;118(2):111–22.
- [34] Wang P, Yi J, Sun C, Luo P, Lei LL. Evaluation of H₂ influence on the evolution mechanism of NO_x storage and reduction over Pt–Ba–Ce/γ-Al₂O₃ catalysts. *Engineering* 2019;5(3):568–75.
- [35] Hu Z, Li KN, Wu XF, Wang N, Li XF, Li Q, et al. Dramatic promotion of visible-light photoreactivity of TiO₂ hollow microspheres towards NO oxidation by introduction of oxygen vacancy. *Appl Catal B* 2019;256:117860.
- [36] Duan YY, Liang L, Lv KL, Li Q, Li M. TiO₂ faceted nanocrystals on the nanofibers: homojunction TiO₂ based Z-scheme photocatalyst for air purification. *Appl Surf Sci* 2018;456:817–26.
- [37] Qian C, Chen W, Li WH, Yu HQ. A chemometric analysis on the fluorescent dissolved organic matter in a full-scale sequencing batch reactor for municipal wastewater treatment. *Front Environ Sci Eng* 2017;11(4):12.
- [38] Pérez T, García-Segura S, El-Ghenemy A, Nava JL, Brillas E. Solar photoelectro-Fenton degradation of the antibiotic metronidazole using a flow plant with a Pt/air-diffusion cell and a CPC photoreactor. *Electrochim Acta* 2015;165:173–81.
- [39] Wang L, Wang JX, Lin JX, Zhang SL, Liu YJ. Degradation of metronidazole by radio frequency discharge in an aqueous solution. *Plasma Processes Polym* 2018;15(4):1700176.